Determination of material properties in the Chaboche unified viscoplasticity model

Q1 **Y P Gong**[1,2]**, C J Hyde**[1]*****,**W Sun**[1]**, and T H Hyde**[1]
[1]Department of Mechanical, Materials and Manufacturing Engineering, University of Nottingham, Nottingham, UK
[2]School of Mechanical Engineering and Automation, Northeastern University, Shenyang, People's Republic of China

Abstract: An experimental programme of cyclic mechanical testing of a 316 stainless steel, at temperatures up to 600 °C, under isothermal conditions, for the identification of material constitutive constants, has been carried out using a thermo-mechanical fatigue (TMF) test machine with induction coil heating. The constitutive model adopted is a modified Chaboche unified viscoplasticity model, which can deal with both cyclic effects, such as combined isotropic and kinematic hardening, and rate-dependent effects, associated with viscoplasticity. The characterization of 316 stainless steel is presented and compared with results from cyclic isothermal tests. A least-squares optimization algorithm has been developed and implemented for determining the material constants in order to further improve the general fit of the model to experimental data, using the initially obtained material constants as the starting point in this optimization process. The model predictions using both the initial and optimized material constants are compared to experimental data.

Keywords: unified viscoplasticity model, 316 stainless steel, material property determination, non-linear least-squares optimization

1 INTRODUCTION

Many components in power generation plant, chemical plant, aeroengines, superplastic forming dies, etc. are subjected to combined mechanical and thermal loading. The materials undergoing these loadings can be working under an inelastic state. An understanding of the material behaviour at high temperature is very important for lifetime estimation of these components. In the last few decades, several viscoplasticity constitutive models have been proposed for predicting material behaviours at high temperature. In 1983, Chaboche [1, 2] put forward what has become known as the unified Chaboche viscoplasticity constitutive model, which has been widely accepted. Phenomena such as cyclic plasticity, creep relaxation, and hardening can be simulated using this model. A key problem for the use of this model is how to determine an initial set of material parameters to be used within the model. A basic method for this initial constant determination has been described by Tong *et al.* [3] and Zhan [4].

Using these initial constants within the model allows a reasonably accurate prediction of the material behaviour; however, a number of greatly simplifying assumptions are made when obtaining these constants. A more accurate material constant set can be obtained by performing an optimization process using this initial constant set as a starting point. This article is particularly concerned with this optimization process and the improvement made to the model, when compared with experimental data, by the optimization. A basic theory for determining optimized material parameters and for model sensitivity of parameters has been proposed by Mahnken and Stein [5], Schwertel and Schinke [6], and Fossum [7, 8]. In this article, Matlab [9] mathematics and optimization toolboxes [10] are used as the development tools for the optimization of the material parameters.

Experimental measurements of cyclic stress–strain loops, within the plasticity and creep ranges, are an essential step towards the determination of material properties for a viscoplasticity model. These equations

*****Corresponding author: Department of Mechanical, Materials and Manufacturing Engineering, University of Nottingham, University Park, Nottingham NG7 2RD, UK.*
email: eaxch@nottingham.ac.uk

can be used in structural analyses aimed at predicting the lives of components such as those in aeroengines and power plant. In this article, the test data obtained from an experimental programme for a 316 stainless steel are presented along with the method used to optimize the material properties.

2 EXPERIMENTAL TESTING

2.1 Materials

All experimental results have been obtained using specimens made of 316 stainless steel. The chemical composition of this material is given in Table 1.

2.2 Test equipment

The thermo-mechanical fatigue (TMF) machine used in this work is an Instron 8862 TMF system, which utilizes radio-frequency induction heating, is shown in Fig. 1, allowing rapid heating. Forced air cooling, through the centre of the specimen, is used, in order to achieve rapid cooling. The maximum achievable load for the machine is 35 kN (limited by the grips) and the maximum allowable temperature is 1100 °C. Figure 2 shows a typical specimen geometry used for testing with this machine. This is the specimen geometry used in obtaining all the test results presented in this article.

2.3 Experimental results

2.3.1 Temperature uniformity

The requirement for temperature uniformity in the gauge section of the specimen during this testing is that the entire gauge section should be within ±10 °C of the target temperature. Therefore, the initial experimental work was concerned with achieving this.

Thermocouples were placed along the gauge section of the specimen in order to monitor the axial, as well as the circumferential, temperature gradients within the specimen gauge section during a series of ramp and hold, as well as cyclic thermal testing. Initially the results were not within this tolerance, with axial deviations of up to ±30 °C from the target temperature. Therefore, new coil designs were investigated.

A key problem faced was achieving the temperature uniformity required while leaving enough space between the turns of the coil for the attachment of the extensometer to the gauge section of the specimen. Figure 1 shows the final coil design which gives temperature uniformity throughout the gauge section
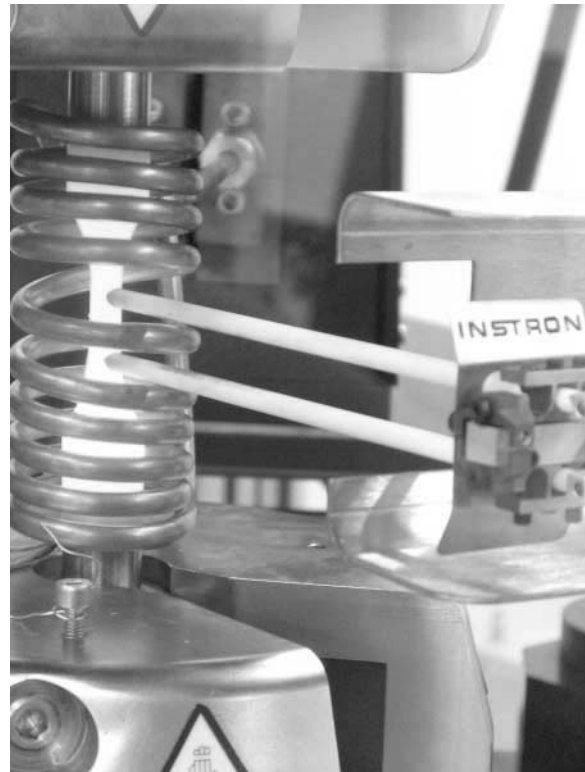

Fig. 1 Photograph of the heated specimen, induction coil, and extensometer setup for the TMF machine

to within the tolerance required for target temperatures ranging from 200 to 1000 °C. Figure 3 shows the temperature uniformity results obtained using this coil and a 316 stainless-steel specimen, for a target temperature of 800 °C.

2.3.2 Isothermal cyclic testing

Isothermal cyclic tests were carried out at temperatures of 300, 500, 550, and 600 °C. At each temperature, the test was performed for 50 cycles (producing 50 loops, shown in Fig. 4) at four strain ranges, i.e. stepped strain-range testing (200 loops in total), using one specimen for each of the temperatures. Example results, at 600 °C, from these tests are shown in Fig. 4. It can be seen that the majority of material hardening occurred at the first and lowest strain range (±0.3 per cent). This can be seen by the large stress difference between the first and second times the maximum strain is reached (for the innermost loops) compared to that of the loops of the three larger strain ranges. Therefore, these test results, at the lowest strain range,

Table 1 Chemical compositions of the 316 stainless steel (wt %)

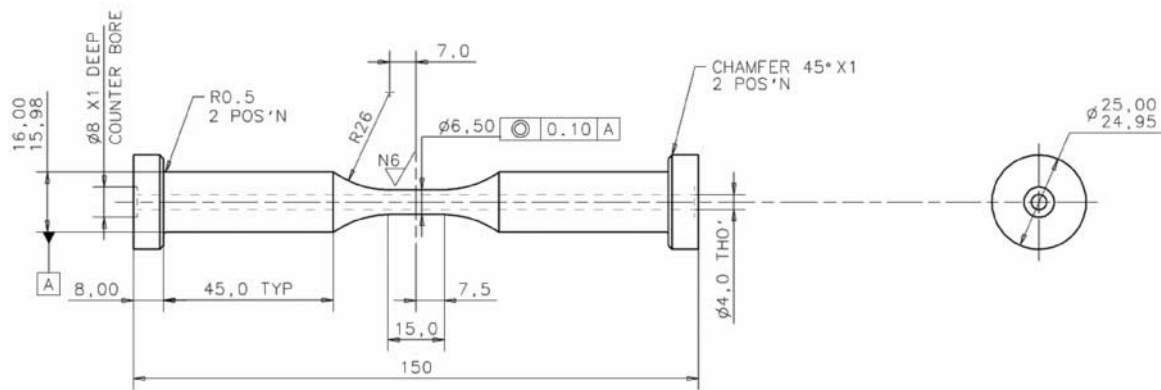| Fe	Cr	Ni	Mo	Mn	Si	Cu	V	Co	S	C	Nb	P	W	Ti	Al
66.4	16.8	11.8	2.15	1.42	0.5	0.49	0.08	0.07	0.03	0.02	0.02	0.01	<0.02	0.01	0.01

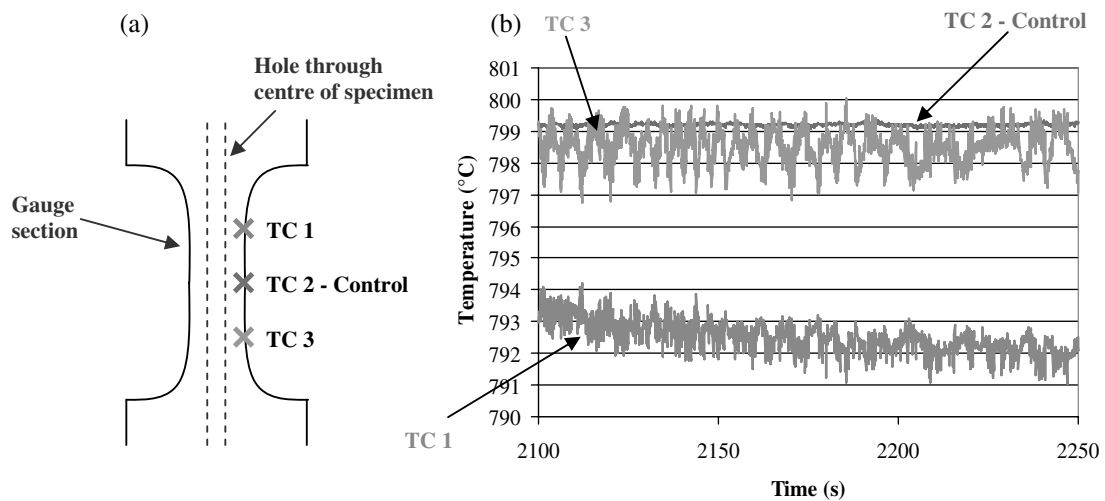**Fig. 2** Specimen geometry used with the TMF machine

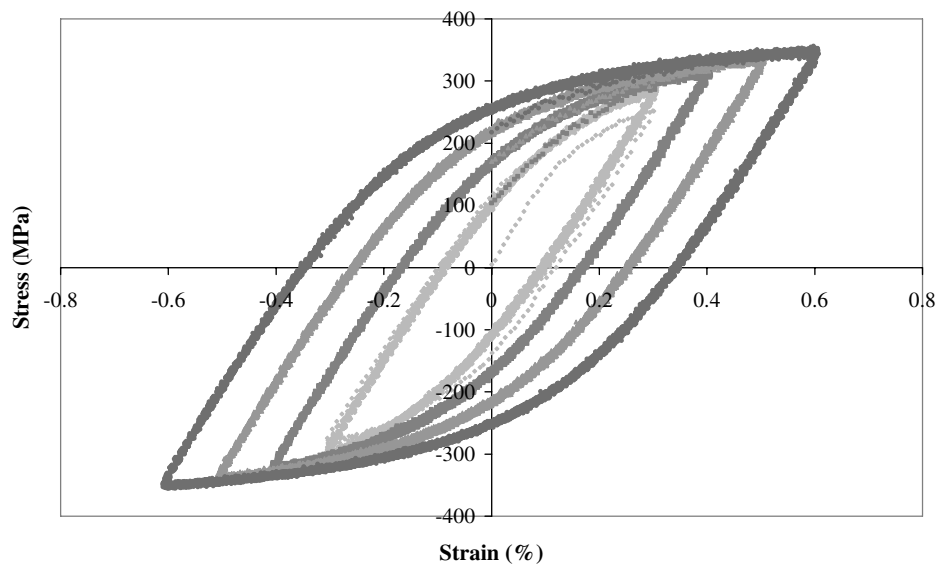**Fig. 3** Thermocouple positions and thermal uniformity results using the final coil

Fig. 4 Isothermal cyclic test results at 600 °C

were used to obtain the material constants for the unified viscoplasticity model for each temperature.

3   THE UNIFIED CYCLIC PLASTICITY AND VISCOPLASTICITY MODEL

The Chaboche unified viscoplasticity model has been chosen to represent the uniaxial cyclic material behaviour of 316 stainless steel. The uniaxial form of the model is as follows

$$\dot{\varepsilon}_p = \left\langle \frac{f}{Z} \right\rangle^n \operatorname{sgn}(\sigma - \chi) \tag{1}$$

where Z and n are material constants, ε_p is the plastic strain, f represents the model yield criterion, shown by the first of the following equations, σ is the stress within the material, calculated as shown by the second of the following equations, and χ is the kinematic hardening parameter.

Also

$$\operatorname{sgn}(x) = \begin{cases} 1 & x > 0 \\ 0 & x = 0 \\ -1 & x < 0 \end{cases} \text{ and } \langle x \rangle = \begin{cases} x & x > 0 \quad x > 0 \\ 0 & x \leqslant 0 \quad x \leqslant 0 \end{cases}$$

The yield criterion and the total stresses are given by

$$f = |\sigma - \chi| - R - k \tag{2}$$

$$\sigma = \chi + (R + k + \sigma_v)\operatorname{sgn}(\sigma - \chi) = E(\varepsilon - \varepsilon_p) \tag{3}$$

where the elastic domain is defined by $f \leqslant 0$ and the inelastic domain by $f > 0$.

The model takes into account both kinematic hardening and isotropic hardening as follows

$$\dot{\chi}_i = C_i(a_i \dot{\varepsilon}_p - \chi_i \dot{p}) \tag{4}$$

$$\chi = \chi_1 + \chi_2 \tag{5}$$

$$\dot{R} = b(Q - R)\dot{p} \tag{6}$$

where $i = 1, 2$, R, and χ are the isotropic and kinematic hardening parameters, respectively, and b, Q, C_i, and a_i are the material constants. p is the accumulative plastic strain, as shown by the following equation

$$\dot{p} = |\dot{\varepsilon}_p| \tag{7}$$

Figure 5 shows the physical meaning of both types of hardening and the effect they have on the yield surface; both types of hardening are shown in three-dimensional (principle) stress space. When the stress state within the material causes the edge of the yield surface to be reached, kinematic hardening, implemented by equations (4) and (5), is represented as the *movement* of the yield surface, as illustrated in Fig. 5(a). Isotropic hardening, implemented by equation (6), represents the *growth* of the yield surface, as shown in Fig. 5(b).

Creep is also accounted for within the model in the form of the Norton [11] creep law as follows

$$\sigma_v = Z\dot{p}^{1/n} \tag{8}$$

Equation (1), the viscoplastic flow rule, is the governing equation within the model. As can be seen from equations (2) to (8), all of the other model variables, such as those used for calculating both types of hardening (isotropic, R, and kinematic, χ) and viscous stress, σ_v, are dependant on the value of accumulated plastic strain, p, calculated in turn as shown by equation (7), from the plastic strain, ε_p, values calculated from this viscoplastic flow rule. Equation (8) defines the viscous stress and therefore the creep effect within the model.

The above model has been implemented in Matlab, which is a high-level programming language.

4   DETERMINATION OF THE INITIAL MATERIAL PROPERTIES

The identification of the final values for material constants requires a step by step procedure. First, the initial values of the parameters are estimated using
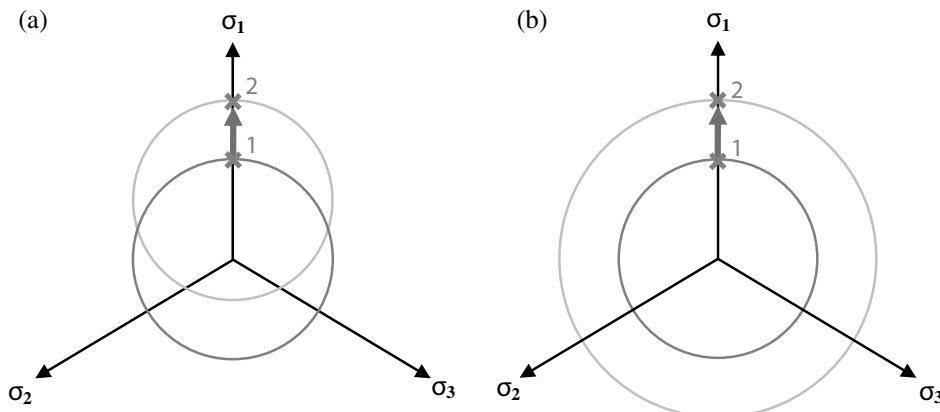

Fig. 5   Schematic representations of hardening behaviour: (a) kinematic and (b) isotropic

the experimental results. These initial values are then used to obtain an optimized material constant set in a simultaneous parameter optimization routine.

In total, the material model requires the identification of ten material constants. This section contains a brief description of the methodologies used in calculating the initial estimations for these constants. The procedure described by Zhan [**4**] is used for estimating the initial values of the isotropic and kinematic hardening constants. However, the initial values for Z and n were determined using a 'trial and error' procedure to fit the experimental data with reference to published literature [**12–15**].

4.1 Initial yield stress, *k*, and Young's modulus, *E*

From the initial (first-quarter cycle) experimental tensile curve, Young's modulus, E, is taken as the gradient of the initial linear region of the curve. The initial yield stress, k, can be estimated as the stress value at the point at which the data begin to deviate from this initial linear region.

4.2 Isotropic hardening parameters, *Q* and *b*

Equation (6) for the rate of isotropic hardening can be integrated with respect to time to give the following equation

$$R = Q(1 - e^{-bp}) \tag{9}$$

$$b = \left[\frac{\ln(1 - R/Q)}{p} \right] \tag{10}$$

Equation (9) shows that as the accumulated plastic strain, p, increases, R exponentially approaches saturation to a value of Q. Therefore, assuming that the material hardening is entirely due to isotropic hardening, and plotting R against the accumulated plastic strain, the saturated value of R is identified as Q, as shown in Fig. 6. Then choosing a point
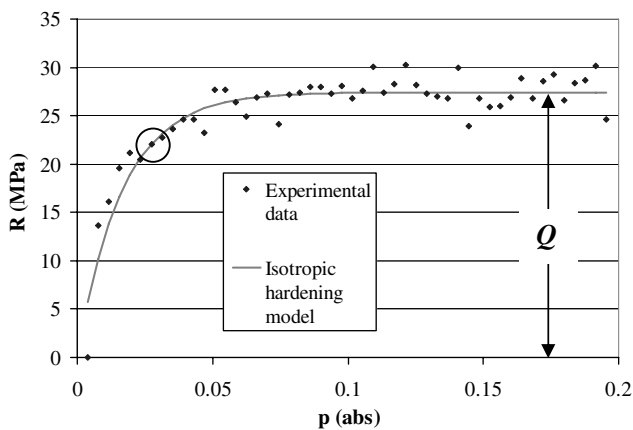

Fig. 6 Isotropic hardening variable R versus p for 316 stainless steel at 600 °C

within the transient region of the hardening behaviour, shown circled in Fig. 6 for example, the corresponding values of R and p can be identified. These values (along with the calculated value of Q) are then put into equation (10), which is a rearranged version of equation (9) for b, and hence b can be identified. By choosing this point roughly half way into the transient region of the hardening behaviour, the calculated value of b 'forces' the model to go through this point, and with the model saturating at the value of Q, the result is a close model fit to the experimental data as shown in Fig. 6.

4.3 Kinematic hardening parameters, a_1, C_1, a_2, and C_2

Equation for the rate of kinematic hardening behaviour can be integrated with respect to time, to give the following equations

$$\chi_1 = a_1(1 - e^{-C_1\varepsilon_p}) \tag{11}$$

$$\chi_2 = a_2(1 - e^{-C_2\varepsilon_p}) \tag{12}$$

If, only the initial tensile curve (first-quarter cycle) is used (therefore, $\sigma - \chi > 0$ and $\text{sgn}(\sigma - \chi) = 1$), equations (11) and (12) can be substituted into equation (5) and then into equation (3) to give

$$\sigma = a_1(1 - e^{-C_1\varepsilon_p}) + a_2(1 - e^{-C_2\varepsilon_p}) + R + k + \sigma_v \tag{13}$$

If the later stages of hardening are considered, it can be assumed that χ_1 (and therefore a_1 and C_1) has a negligible effect on the hardening and therefore the kinematic hardening is dominated by χ^2 (a_2 and C_2). Therefore, equation (13) can be simplified to

$$\sigma = a_2(1 - e^{-C_2\varepsilon_p}) + R + k + \sigma_v \tag{14}$$

Differentiating equation (14) with respect to ε_p, rearranging and taking natural logs of both sides gives the following equation (assuming yield stress, k, and viscous stress, σ_v, to be constants)

$$\ln\left(\frac{\partial\sigma}{\partial\varepsilon_p} - \frac{\partial R}{\partial\varepsilon_p}\right) = -C_2\varepsilon_p + \ln(a_2 C_2) \tag{15}$$

Therefore, plotting $\ln[(\partial\sigma/\partial\varepsilon_p) - (\partial R/\partial\varepsilon_p)]$ versus ε_p as shown in Fig. 7 allows the identification of C_2 from the gradient, and a_2 from the y-axis intercept. Similarly, a_1 and C_1 can be found for the lower strain region, from equation (13), having already identified a_2 and C_2 [**4**].

In order to perform this fit to the data, it is necessary to obtain expressions for $\partial\sigma/\partial\varepsilon_p$ and $\partial R/\partial\varepsilon_p$, as functions of ε_p, to use in equation (15). For the initial tensile curve (the first quarter cycle), $p = \varepsilon_p$, which can
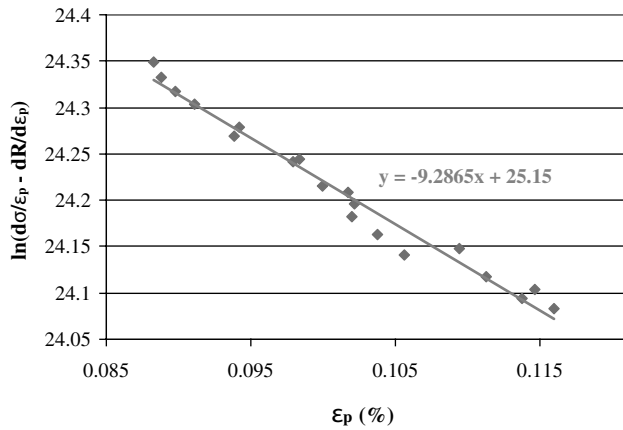
Fig. 7 Plot used in the calculation of the kinematic hardening material constants a_2 and C_2 for 316 stainless steel at 600 °C

be substituted into equation (9). This expression can then be differentiated with respect to ε_p, to give the following

$$\frac{\partial R}{\partial \varepsilon_p} = bQ\mathrm{e}^{-b\varepsilon_p} \tag{16}$$

The calculation of $\partial\sigma/\partial\varepsilon_p$ is more complicated. Taking $\mathrm{d}\sigma/\mathrm{d}\varepsilon_p$, multiplying by $\mathrm{d}t/\mathrm{d}t$ and $\mathrm{d}\varepsilon_T/\mathrm{d}\varepsilon_T$, then rearranging gives the following

$$\frac{\mathrm{d}\sigma}{\mathrm{d}\varepsilon_p} = \frac{\mathrm{d}\sigma}{\mathrm{d}\varepsilon_T}\frac{1}{\dot{\varepsilon}_p}\dot{\varepsilon}_T \tag{17}$$

Hence, expressions for $\mathrm{d}\sigma/\mathrm{d}\varepsilon_T$ and $\dot{\varepsilon}_p$ are required. The value of $\dot{\varepsilon}_T$ is controlled during testing and hence is known. To obtain $\dot{\varepsilon}_p$, Hooke's law, $\varepsilon_e = \sigma/E$, is substituted into the following equation for total strain

$$\varepsilon_T = \varepsilon_e + \varepsilon_p \tag{18}$$

$$\varepsilon_T = \frac{\sigma}{E} + \varepsilon_p \tag{19}$$

Rearranging equation (18) and differentiating it with respect to time gives

$$\frac{\mathrm{d}\varepsilon_p}{\mathrm{d}t} = \frac{\mathrm{d}\varepsilon_T}{\mathrm{d}t} - \frac{\mathrm{d}\sigma}{\mathrm{d}t}\frac{1}{E} \tag{20}$$

Multiplying the final term in equation (20) by $\mathrm{d}\varepsilon_T/\mathrm{d}\varepsilon_T$ and rearranging gives

$$\dot{\varepsilon}_p = \dot{\varepsilon}_T\left(1 - \frac{1}{E}\frac{\mathrm{d}\sigma}{\mathrm{d}\varepsilon_T}\right) \tag{21}$$

Therefore, an expression for $\mathrm{d}\sigma/\mathrm{d}\varepsilon_T$ is needed in equations (17) and (21). In order to obtain an expression for $\mathrm{d}\sigma/\mathrm{d}\varepsilon_T$, a smoothing function is needed to eliminate complications caused by scatter in the experimental data, which could cause negative values of $\mathrm{d}\sigma/\mathrm{d}\varepsilon_T$ to be obtained at some strain values.

The smoothing function used in this case is the Ramberg–Osgood equation [16–18], that is

$$\frac{\varepsilon_T}{\varepsilon_0} = \frac{\sigma}{\sigma_0} + \left(\frac{\sigma}{\sigma_0}\right)^{n_0} \tag{22}$$

$$\varepsilon_0 = \frac{\sigma_0}{E} \tag{23}$$

Equation (23) can be substituted into equation (22) to give

$$\frac{E\varepsilon_T}{\sigma_0} = \frac{\sigma}{\sigma_0} + \left(\frac{\sigma}{\sigma_0}\right)^{n_0} \tag{24}$$

which can then be differentiated with respect to ε_T to give

$$\frac{\mathrm{d}\sigma}{\mathrm{d}\varepsilon_T} = \frac{\sigma_0}{\varepsilon_0\left[1 + n_0\left(\sigma/\sigma_0\right)^{n_0-1}\right]} \tag{25}$$

The Ramberg–Osgood constants, namely ε_0, σ_0, and n_0, can be found by rearranging and taking logs of both sides of equation (24) to give

$$\log(E\varepsilon_T - \sigma) = n_0\log\sigma + (1 - n_0)\log\sigma_0 \tag{26}$$

Therefore, plotting $\log(E\varepsilon_T - \sigma)$ versus $\log\sigma$ allows the identification of n_0 (gradient) and σ_0 (from the y-axis intercept). An example of this plot, for a temperature of 600 °C, is shown by Fig. 8. Equation (23) can then be used to determine ε_0. Table 2 shows the Ramberg–Osgood constants calculated for the four temperatures.
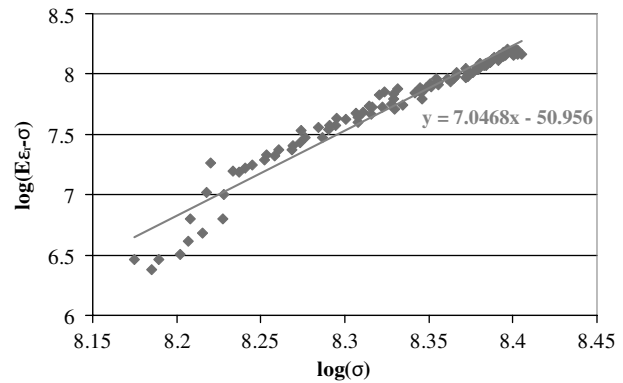

Fig. 8 Plot of $\log(E\varepsilon_T - \sigma)$ versus $\log\sigma$ used in determining the constants used in the Ramberg–Osgood equation

Table 2 Ramberg–Osgood constants at multiple temperatures

T (°C)	ε_0 (%)	σ_0 (MPa)	n_0
300	0.218 03	337.61	7.2409
500	0.202 77	295.11	6.1627
550	0.217 79	307.65	7.2846
600	0.192 12	267.26	7.0468

4.4 Creep constants, Z and n

Typical values of Z and n have been taken from the literature, such as Ryu [12] and Hyde [13–15]. The Matlab computer program for the model was run varying these constants within the typical range of values in order to obtain good fits to the model; this resulted in the constants presented in Table 3.

4.5 Initial material constants

Table 2 summarizes the initial material constants identified from the isothermal test data for 316 stainless steel for the four temperatures.

5 OPTIMIZATION OF THE MATERIAL CONSTANTS

5.1 Optimization model

The identification of the material constants in the Chaboche unified viscoplasticity model is a reverse process based on experimental data. In order to accurately determine the full set of material constants, an optimization procedure is adopted. The optimization method selected is a least-squares algorithm. The principle of the optimization is to search for the global minimum of the difference between the square sum of the calculated stresses from the Chaboche model and the corresponding measured stresses obtained from strain-controlled cyclic experimental data [5]. The optimization model can be described mathematically as

$$F(\boldsymbol{x}) = \frac{1}{2} \sum_{i=1}^{M} [\sigma(x)_i^{\text{pre}} - \sigma_i^{\text{exp}}]^2 \rightarrow \min \qquad (27)$$

$$x \in R^n \qquad (28)$$

$$\text{LB} \leqslant x \leqslant \text{UB} \qquad (29)$$

where $F(\boldsymbol{x})$ is the objective function, $\boldsymbol{x}$ is the optimization variable set (a vector of n-dimensional space, R^n), which for this specific case contains the full set of material constants in the Chaboche model

$$\boldsymbol{x} = [a_1, c_1, a_2, c_2, z, n, b, Q, k, E]^{\text{T}} \qquad (30)$$

LB and UB are the lower and upper boundaries of $\boldsymbol{x}$ allowed during the optimization. $\sigma(\boldsymbol{x})_i^{\text{pre}}$ and σ_i^{exp} are the model predicted total stress and the experimental measured stress, respectively, at a specific

time i, within the loops. M is the total number of experimental data points used in the optimization.

5.2 Numerical techniques

At a specific point within the stress–strain loops, the predicted total stress $\sigma(x)_i^{\text{pre}}$ can be obtained by solving a set of differential equations, as shown in equations (1) to (8), for a known material constant set, $\boldsymbol{x}$. The total stress rate is given by

$$\dot{\sigma} = E(\dot{\varepsilon} - \dot{\varepsilon}_{\text{p}}) \qquad (31)$$

From equations (1) to (8) and equation (31) a first-order non-linear system of differential equations with the variables of ε_{p}, χ_1, χ_2, R, and σ can be obtained. To calculate the predicted stress value, $\sigma(x)_i^{\text{pre}}$, it is necessary to solve the system of differential equations using a numerical method. This involves obtaining numerical solutions for the following state vector

$$\boldsymbol{y} = [\varepsilon_{\text{p}}, \chi_1, \chi_2, R, \sigma]^{\text{T}} \qquad (32)$$

One of the most popular methods of solving differential equations using numerical techniques is the automatic adaptive variable step Runge–Kutta–Fehlberg algorithm [19]. For each time interval, the updated state vector, $\boldsymbol{y}_{m+1}$, at the $(m+1)$th time step, is estimated as

$$\boldsymbol{y}_{m+1} = \boldsymbol{y}_m + \sum_{j=1}^{6} \gamma_j k_j \qquad (33)$$

A tolerance vector, $\boldsymbol{e}_m$, is introduced to estimate the variation sensitivity of the solution to the step length

$$\boldsymbol{e}_m = \sum_{j=1}^{6} (\gamma_j - \gamma_j^*) k_j \qquad (34)$$

The next time step increment can be adjusted based on the current value of $\boldsymbol{e}_m$. γ_j and γ_j^* are algorithm factors, and the values of variable k_j is calculated in the Runge–Kutta–Fehlberg algorithm [19].

5.3 Implementation in Matlab

Matlab is a high-performance language for technical programming and computing. Various toolboxes are provided within Matlab, including the Mathematics

Table 3 Initial material constants at multiple temperatures

T (°C)	k (MPa)	E (GPa)	b	Q (MPa)	a_1 (MPa)	C_1	a_2 (MPa)	C_2	Z (MPa.s$^{1/n}$)	N
300	39	154.84	39.46	32.76	119.1	5964.1	108.4	1001.6	179	10
500	32.5	145.54	33.35	30.41	94.6	6472.6	113.3	979.91	175	10
550	31	141.26	31	27.8	86.3	6939	114.8	957.69	173	10
600	30	139.12	28.6	27.43	80.06	7111.9	116	928.7	170	10

Toolbox and Optimization Toolbox, which extends the capability of the Matlab numeric computing environment and has access to most of the standard routines within Matlab [**9, 10**].

The ODE45 function within the Matlab Mathematics Toolbox has been selected for solving the first-order system of differential equations from the initial values problem. A variable step length Runge–Kutta–Fehlberg algorithm is utilized within the ODE45 function. From the initial value of $\boldsymbol{y}_o$ and the time interval beginning at t_0 and ending at t_{final}, i.e. $[t_o, t_{\text{final}}]$, the value of the state vector shown by equation (32) can be obtained for a given set of material parameters, i.e. the optimization variable set, $\boldsymbol{x}$.

The non-linear least-squares optimization function **lsqnonlin** is provided within the Matlab optimization Toolbox, in which the Levenberg–Marquardt algorithm is used for each of the iteration steps. Gradient matrix and Jacobian matrix of the objective function, $F(\boldsymbol{x})$, are unnecessary to be provided in explicit form. They can be calculated automatically within the **lsqnonlin** function using the finite difference method.

5.4 Program development

An optimization program for determining the material parameters in the Chaboche unified viscoplasticity model has been developed and implemented within Matlab. It is very convenient to utilize the Matlab functions to solve the differential equations and to process the results using Matlab. Figure 9 shows the
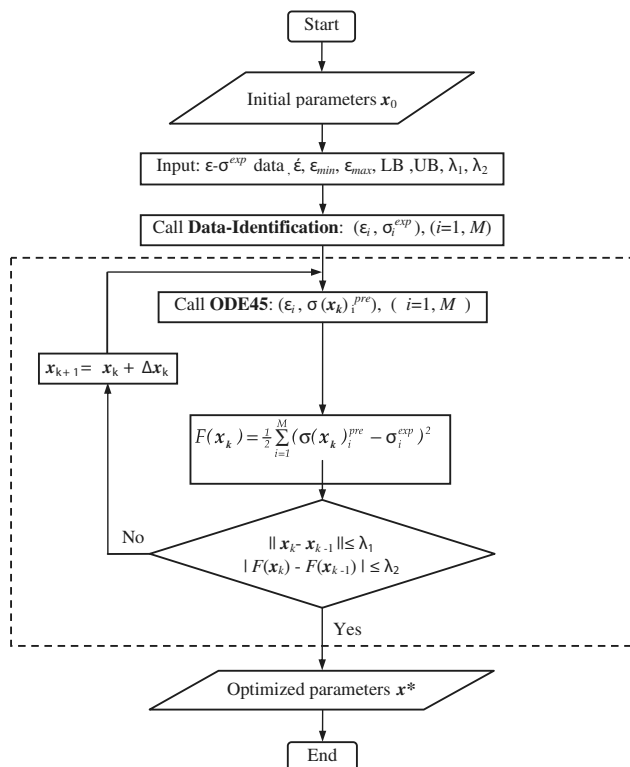

Fig. 9 Flowchart for the optimization process

flowchart for the optimization process implemented within Matlab, where the dashed box highlights the **lsqnonlin** optimization process.

The initial parameters estimated using the experimental data are used as the input in a simultaneous identification procedure within the optimization.

In order to reduce the computing time of the iterative seeking process, a user-defined subroutine, **Data-Identification**, for the identification and selection of experiment data has been developed within Matlab and a series of subintervals of time can be obtained from the experimental loops. The predicted stress value at the end point of a subinterval is calculated using the ODE45 function corresponding to a certain set of material parameters $\boldsymbol{x}_k$.

Within the **lsqnonlin** optimization function, the optimization process is implemented and the optimum parameters, $\boldsymbol{x}^*$, are obtained. In order to avoid convergencing to a local minimum rather than to the intended global minimum, the first step was to obtain the first set of 'optimum' parameters, by the least-squares method starting from the initially estimated sets of parameters. These sets of optimum parameters are then perturbed by adjusting a finite step away from it to investigate whether a better minimum is achieved or whether it returns to the same position. This process is repeated until the same minimum is returned from different restart positions.

Calculated results obtained directly from the Chaboche model using the differential equation solver within the Matlab are compared with those obtained from a time marching method. Encouragingly, the two sets of results are almost identical. Some discrete data obtained from a theoretical function are also used to check the validation of the optimization program. Again the same level of accuracy was obtained.

5.5 Optimized constants

Table 4 summarizes the optimized material constants using the initial material constants (Table 3) as the starting points for the optimization process.

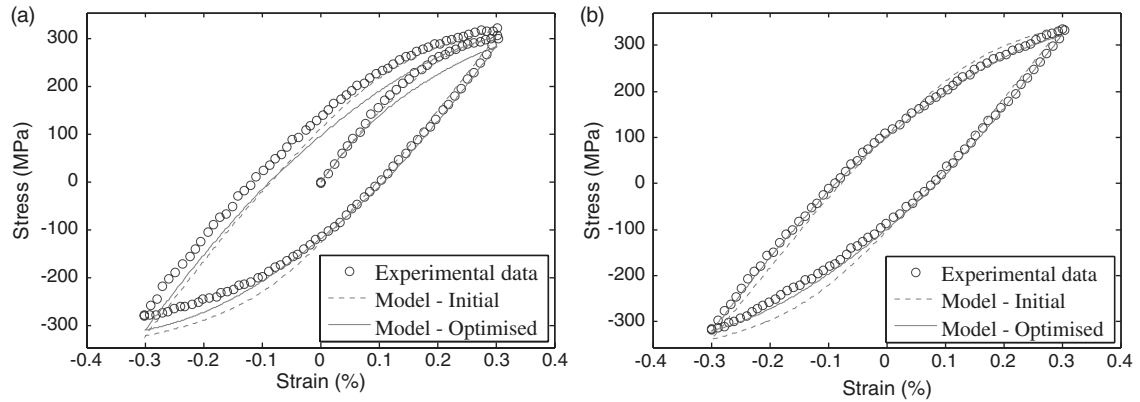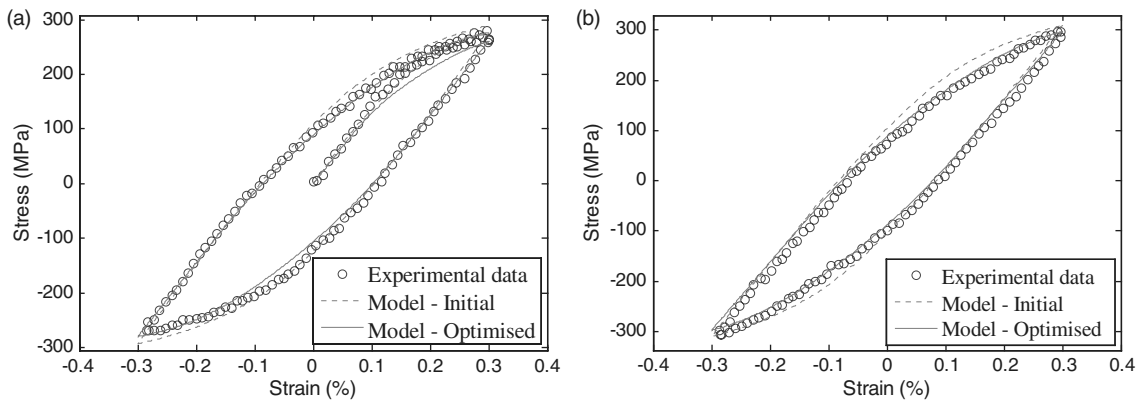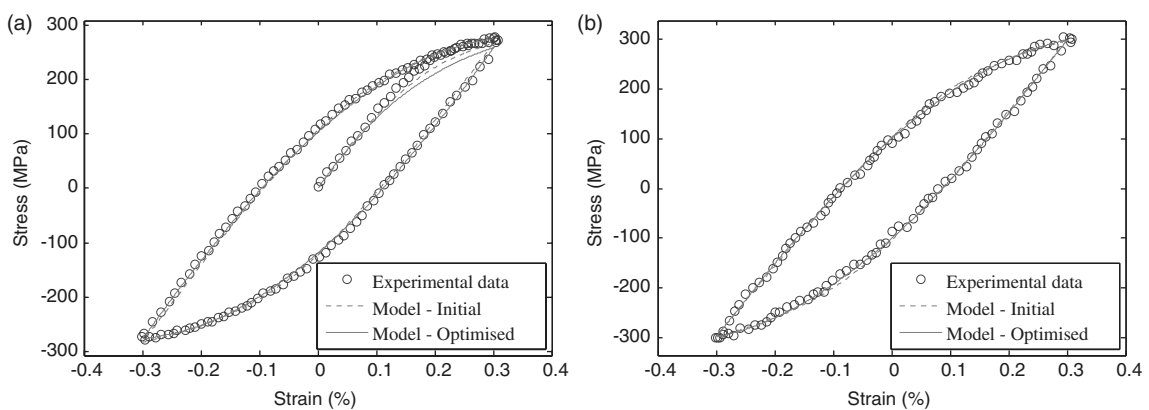## 6 COMPARISON OF MODEL AND EXPERIMENTAL DATA

Figures 10 to 14 show comparisons of the material model predictions and the experimental data for a range of temperatures, using both the initial and the optimized material constants.

6.1 Initial and stabilized loops

Within this section, for all of the figures shown, part (a) shows the initial tensile curve and first full loop for the relevant temperature. Each part (b) shows the stabilized loop for the same temperature as the corresponding part (a).

Table 4 Optimized material constants at multiple temperatures

T (°C)	k (MPa)	E (GPa)	B	Q (MPa)	a_1 (MPa)	C_1	a_2 (MPa)	C_2	Z (MPa.s$^{1/n}$)	n
300	28.99	159.0655	19.92	26.79	55.47	16 343.09	211.22	1215.40	116.06	7.21
500	37.98	135.4666	16.77	32.79	36.66	19 963.66	160.59	1506.58	70.60	40.00
550	27.29	146.9359	11.29	36.93	70.17	11 744.56	171.01	1396.05	39.72	11.38
600	18.98	149.6897	42.45	28.68	87.56	7285.09	163.53	1328.70	129.12	3.72

Fig. 10 Model comparison to experimental data using both the initial and optimized material constants at 300 °C: (a) initial tensile curve and first loop and (b) saturated loop

Fig. 11 Model comparison to experimental data using both the initial and optimized material constants at 500 °C: (a) initial tensile curve and first loop and (b) saturated loop

Fig. 12 Model comparison to experimental data using both the initial and optimized material constants at 550 °C: (a) initial tensile curve and first loop and (b) saturated loop
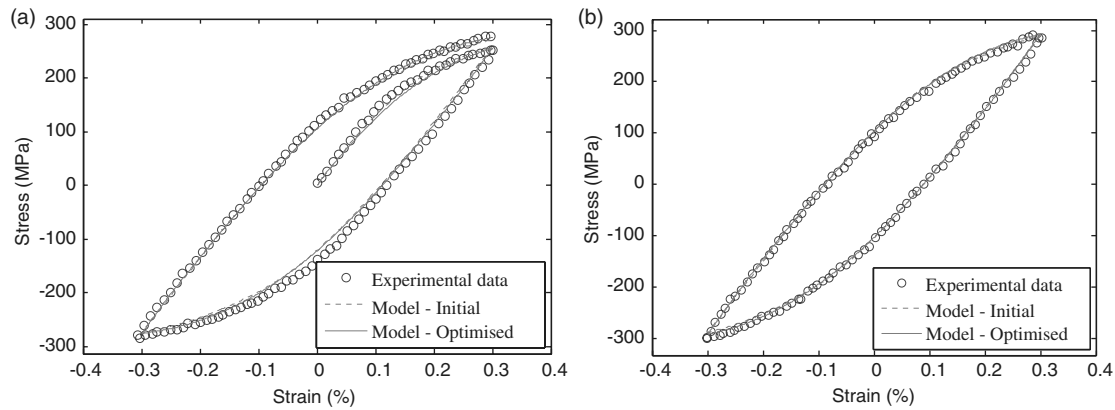
Fig. 13 Model comparison to experimental data using both the initial and optimized material constants at 600 °C: (a) initial tensile curve and first loop and (b) saturated loop
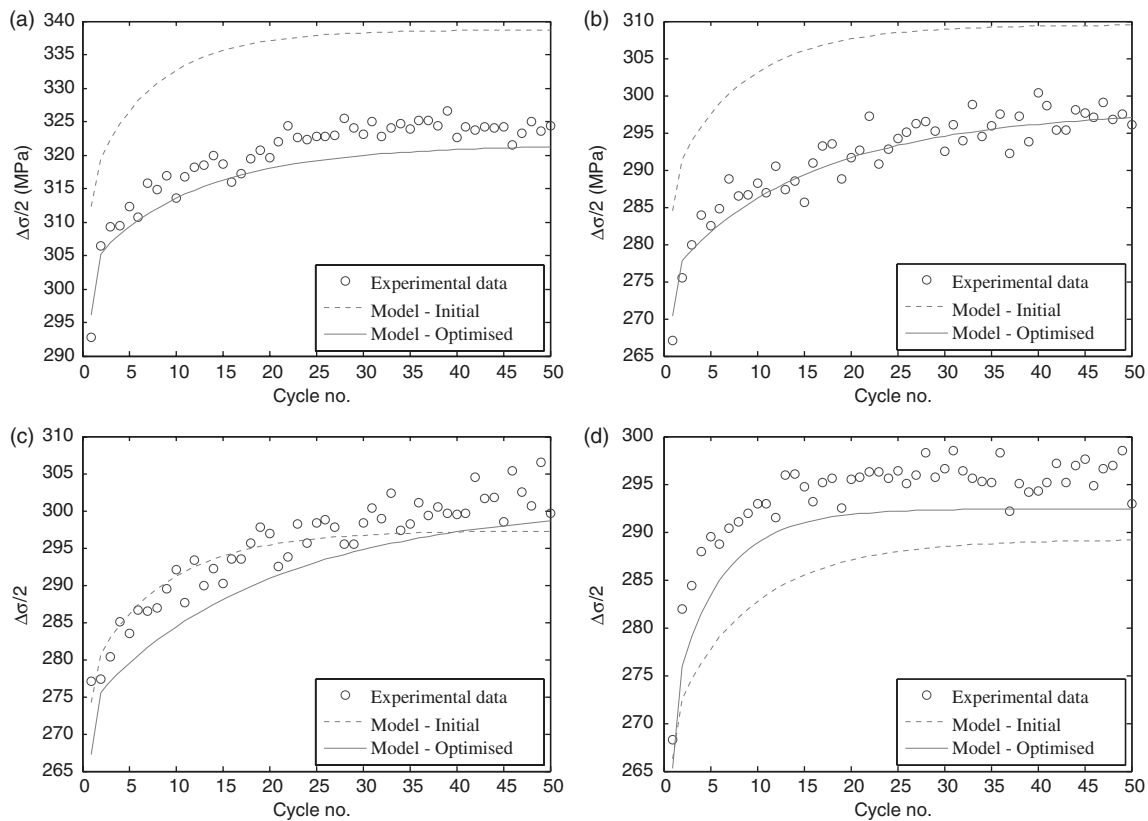

Fig. 14 Model comparison to experimental data using both the initial and optimized material constants for hardening behaviour at (a) 300 °C, (b) 500 °C, (c) 550 °C, and (d) 600 °C

6.2 Hardening behaviour

Within this section, the hardening behaviour for each temperature is presented.

7 DISCUSSION AND FUTURE WORK

A unified viscoplasticity material model, which includes both (non-linear) isotropic and kinematic hardening behaviour as well as viscoplasticity phenomena, such as rate dependency, has been implemented in Matlab. A programme of isothermal tests has been conducted using induction coil heating, with the temperature uniformity controlled to within ±10 °C up to temperatures of 600 °C. The test data have been used to identify the material constants for the material model at different temperatures between 300 and 600 °C. The experimental data have also been

employed to validate the Matlab implementation of the unified viscoplasticity model, showing excellent model to test correlation for the isothermal tests considered.

Although the material constants obtained directly from the experimental data give fairly accurate predictions of the material behaviour when compared with the experimental data, some fairly crude assumptions have to be made. Such an assumption includes that the kinematic constants a_1 and C_1 have negligible effect on the hardening behaviour at high strain values in order to obtain a_2 and C_2. Therefore, the employment of an optimization scheme, which was developed within this work, has been used to obtain a new set of material constants. The starting point for the optimization procedure is the initial constants obtained directly from the experimental data. This new set of material constants gives a more accurate prediction of the material behaviour, when compared with the experimental data, than the initial estimation. The optimization method used is based on a least-squares algorithm. Within the optimization, the global minimum of the difference between the square sum of the calculated stresses from the model and the corresponding measured stresses obtained from strain-controlled cyclic experimental loops is searched for, in order to provide the best general fit to the experimental data. The implementation of this optimization process has proven to further improve the general fit of the model to experimental data.

This work will be further developed in order that relaxation periods can be included at the extreme strains within the mechanical waveforms. Another area for intended future development is the implementation of temperature dependency of the model in order that TMF simulations can be run and compared to corresponding experimental data.

ACKNOWLEDGEMENTS

REFERENCES

1 **Chaboche, J. L.** and **Rousselier, G.** On the plastic and viscoplastic constitutive equations – part 1: rules developed with internal variable concept. *J. Press. Vessel Technol.*, 1983, **105**, 153–158.
2 **Chaboche, J. L.** and **Rousselier, G.** On the plastic and viscoplastic constitutive equations – part 2: application of internal variable concepts to the 316 stainless steel. *J. Press. Vessel Technol.*, 1983, **105**, 159–164.
3 **Tong, J., Zhan, Z. L.,** and **Vermeulen, B.** Modelling of cyclic plasticity and viscoplasticity of a nickel-based alloy using Chaboche constitutive equations. *Int. J. Fatigue*, 2004, **26**(8), 829–837.
4 **Zhan, Z.** A study of creep-fatigue interaction in a new nickel-based superalloy. PhD Thesis, University of Portsmouth, 2004.
5 **Mahnken, R.** and **Stein, E.** Parameter identification for viscoplastic model based on analytical derivatives of a least-squares functional and stability investigations. *Int. J. Plast.*, 1996, **12**(4), 451–479.
6 **Schwertel, J.** and **Schinke, B.** Automated evaluation of material parameters of viscoplastic constitutive equations. *Trans. ASME, J. Eng. Mater. Technol.*, 1996, **118**, 273–280.
7 **Fossum, A. F.** Parameter estimation for an internal variable model using nonlinear optimisation and analytical/numerical response sensitivities. *Trans. ASME, J. Eng. Mater. Technol.*, 1997, **119**, 337–345.
8 **Fossum, A. F.** Rate data and material parameter estimation. *Trans. ASME J. Eng. Mater. Technol.*, 1998, **120**, 7–12.
9 T. M. Inc, Matlab 7 Mathematics, 2008.
10 T. M. Inc, Optimisation toolboxTM 4 User's guide, 2008.
11 **Norton, F. H.** *The creep of steel at high temperature*, 1929 (McGraw Hill, New York).
12 **Ryu, W.-S., Kim, W. G., Lee, K. Y.,** and **Yoon, K. B.** *Evaluation of Creep Crack Growth Behaviour in Type 316LN Stainless Steel*, Manuscript for SMiRT 17 – NED Special Issue, Korea.
13 **Hyde, T. H.** Creep crack growth in 316 stainless steel at 600 °C. *High Temp. Technol.* 1988, **6**(2), 51–61.
14 **Hyde, T. H.** Anomalous creep behaviour of 316 stainless steel at 550 °C. *High Temp. Technol.*, 1986, **4**(1), 25–29.
15 **Hyde, T. H.** Creep of 316 stainless steel at 550 and 600 °C and the effects of short duration overloads on creep at 550 °C. *Mater. High Temp.*, 1997, **14**(1), 27–35.
16 **Ramberg, W.** and **Osgood, W.** *Description of stress–strain curves by three parameters*, 1943, p. 902 (NASA Scientific and Technical Information Facility, Washington).
17 **Hill, H. N.** *Determination of stress-strain relations from 'offset' yield strength values*, 1944, p. 927 (Aluminium Company of America, Washington).
18 **Rasmussen, K. J. R.** *Full-range stress–strain curves for stainless steel alloys*, 2001, p. R811 (Department of Civil Engineering, University of Sydney, Sydney).
19 **Gerald, C. F.** and **Wheatley, P. O.** *Applied numerical analysis*, 1999 (Addison-Weslrey).   Q2

JMDA273

Queries

Y P Gong, C J Hyde, W Sun, and T H Hyde

Q1   There is a discrepancy for the corresponding author initial between the Cover sheet and the doc file. We
      have followed the one given in the doc file. Please check.

Q2   Please provide place of publication in reference [**19**].